

Effect of Stress Relief Annealing on Microstructure & Mechanical Properties of Welded Joints Between Low Alloy Carbon Steel and Stainless Steel



R. NIVAS, G. DAS, S.K. DAS, B. MAHATO, S. KUMAR, K. SIVAPRASAD, P.K. SINGH, and M. GHOSH

Two types of welded joints were prepared using low alloy carbon steel and austenitic stainless steel as base materials. In one variety, buttering material and weld metal were Inconel 82. In another type, buttering material and weld metal were Inconel 182. In case of Inconel 82, method of welding was GTAW. For Inconel 182, welding was done by SMAW technique. For one set of each joints after buttering, stress relief annealing was done at ~ 923 K (650 °C) for 90 minutes before further joining with weld metal. Microstructural investigation and sub-size *in situ* tensile testing in scanning electron microscope were carried out for buttered-welded and buttered-stress relieved-welded specimens. Adjacent to fusion boundary, heat-affected zone of low alloy steel consisted of ferrite-pearlite phase combination. Immediately after fusion boundary in low alloy steel side, there was increase in matrix grain size. Same trend was observed in the region of austenitic stainless steel that was close to fusion boundary between weld metal-stainless steel. Close to interface between low alloy steel-buttering material, the region contained martensite, Type-I boundary and Type-II boundary. Peak hardness was obtained close to fusion boundary between low alloy steel and buttering material. In this respect, a minimum hardness was observed within buttering material. The peak hardness was shifted toward buttering material after stress relief annealing. During tensile testing no deformation occurred within low alloy steel and failure was completely through buttering material. Crack initiated near fusion boundary between low alloy steel-buttering material for welded specimens and the same shifted away from fusion boundary for stress relieved annealed specimens. This observation was at par with the characteristics of microhardness profile. In as welded condition, joints fabricated with Inconel 82 exhibited superior bond strength than the weld produced with Inconel 182. Stress relief annealing reduced the strength of transition joints and the reduction was maximum for specimen welded with Inconel 82.

DOI: 10.1007/s11661-016-3840-9

© The Minerals, Metals & Materials Society and ASM International 2016

I. INTRODUCTION

WELDING is the most preferred process when it comes to permanent joining of metals for a wide range of industrial applications. Dissimilar metal welding (DMW) is one of the key areas that extends the versatility of the process. Low alloy steels are widely used in low temperature zone of power generation plant. On the other hand, high temperature regions require materials like austenitic alloys for superior corrosion

resistance and greater creep strength.^[1,2] In a typical nuclear power plant, there can be thousands of DMWs, which experience numerous thermal cycling between room temperature and ~ 623 K (350 °C).^[3-5] One of the examples is weld joint between low alloy steel (LAS) and austenitic stainless steel (ASS). The nozzle material is ASTM A508 Grade 3 Class 1 (low alloy steel) and connecting piping material is SA312-Type 304LN (austenitic stainless steel). This transition joint is widely used as primary piping of heat transport system in pressurized water reactors (PWR) of nuclear power plants.^[3]

Besides its unique application, a lot of mechanical and metallurgical hurdles are associated with it. The weld thermal cycle produces heat-affected zone (HAZ) and weld nugget, containing heterogeneous microstructure.^[1,5,8] The constitution of joining is critical, because any deviation out of optimum window may lead to deleterious weld due to embrittlement and/or hot/cold cracking. Several factors are collectively responsible for premature failure of such dissimilar metal weld.^[6] During fabrication to reduce detrimental effects, different types of welding consumables are introduced.

R. NIVAS, M.Tech. Student, and K. SIVAPRASAD, Assistant Professor, are with the Advanced Materials Processing Laboratory, Department of Metallurgical and Materials Engineering, National Institute of Technology, Tiruchirappalli 620015, India. G. DAS, Sr. Principal Scientist, S.K. DAS, Principal Scientist, B. MAHATO, Technical Officer, and M. GHOSH, Sr. Scientist, are with the Material Science & Technology Division, CSIR-National Metallurgical Laboratory, Jamshedpur 831007, India. Contact e-mail: ghosh_mnk@yahoo.com S. KUMAR, Scientific Officer 'D', and P.K. SINGH, Scientific Officer 'G', are with the Reactor Safety Division, Bhabha Atomic Research Centre, Mumbai 400085, India.

Manuscript submitted May 2, 2016.

Article published online October 27, 2016

Inconel welding wires are used to join LAS components to ASS pipes. Inconel wires are promising candidates to minimize the differences in composition and thermal expansion of two different metals.^[9–11] Ni-base alloys have an additional advantage of restricting carbon diffusion from low alloy to stainless steel as diffusivity of carbon is very low in face-centered cubic nickel compared with stainless steel.^[7] Carbon migration leads to form localized carbon-depleted soft zone and carbon-rich hard zone across fusion boundary. This makes whole region prone to degeneration during service exposure.^[3]

Concern and interest in the integrity of dissimilar metal welds were raised since the cracking incident in V.C. Summer nuclear power plant, which took place in the year 2000. In that incident, through wall cracking in Inconel 82/182 weld of hot leg nozzle, primary water leaked out.^[12] Failure investigation of the weld consisting of ferritic and austenitic stainless steel was carried out by Samal *et al.*^[13] using single edge-notched bend specimens with initial cracks machined at different locations. In fabricating those joints, E309L and E308L were used as buttering material and weld metal, respectively. It was concluded that the fracture resistance of joint was low because of micro-cracking at fusion boundary and presence of HAZ at edge. Embrittlement across fusion boundary was contributed by martensitic transformation and stress generation.^[3,14] This was endorsed by sharp rise in hardness near fusion boundary for welded joint consisting of T91/347H steel combination.^[15] In that case, IN82 (ERNiCr-3) was used as a filler material. It was highlighted that highest UTS was corresponded to the sample welded by GTAW process.^[15] To improve the joint quality, Rathod *et al.*^[3] have suggested deposition of Ni-Fe alloy (ERNiFe-CI 1) as first layer for buttering. This might be followed by the deposition of Inconel 82 as subsequent layers. In that study, carbon concentration did not suffer a drastic change at interface and diffusion of carbon was reduced in the temperature range of ambient to ~723 K (450 °C). In another investigation, ferritic steel was welded with austenitic stainless steel using different filler materials.^[11] Four consumables, *i.e.*, 316 SS, 16-8-2, Inconel 82 (IN82), and Inconel 182, (IN182) were considered for the study. Apart from providing adequate solidification cracking resistance, Inconel filler materials were preferable over others considering its adequate mechanical property and intermediate coefficient of thermal expansion. Local variations in mechanical properties of dissimilar weld produced between SA508 and F316SS using IN82/182 were investigated at room temperature and ~623 K (350 °C).^[15] It was reported that the minimum ductility was obtained at HAZ for both joints at both temperatures. A significant change in uniform elongation and stress associated with plastic instability for joints were reported. Variation in mechanical properties for joints consisting of low alloy steel-316SS using IN82/182 weld metal was studied by Jang *et al.*^[16] It was reported that ultimate tensile strength and fracture toughness of weld were 50 to 70 MPa and 70 pct greater near top in comparison to bottom, respectively. It was concluded that the variation came from synergistic effect

of composition, microstructure, and thermomechanical history during multi-pass welding of thick plates. Ming *et al.* have performed structural characterization of welded joint between SA508 and 316L SS using 309L SS as buttering material and 308L SS as weld metal.^[17] Delta ferrite along grain boundaries of 316L SS was observed. Similar type of investigation was carried out by Pan and Zhang to explore the structural heterogeneities across fusion boundary.^[18]

Dissimilar materials weld consisting of ferritic and austenitic stainless steel plate with thickness ~6 mm was fabricated through CO₂ laser beam welding without using filler metal.^[19,20] Microstructural study was carried out along with evaluation of mechanical properties. Weld region of dissimilar material contained inhomogeneous microstructure of ferrite/austenite + bainite and/or martensite due to incomplete mixing of two alloys in molten state. Solidification cracking parallel to dendritic growth was found. HAZ of St32-austenitic stainless contained no martensite, however, the same region of St52-austenitic steel showed the presence of martensite. Peak hardness was reported in the range of 380 to 400 Hv for St37-austenitic stainless steel within weld and ~425 Hv within ferrite for St52-austenitic stainless steel joint. Tensile testing of specimen taken from transverse section exhibited failure from weak ferritic steel. Evaluation of local tensile properties using micro-tensile specimens revealed high strength at weld metal and heat-affected zone of ferrite. Heat-affected zone of austenite did not show any significant change. Fracture surface of tensile specimens revealed ductile dimple fracture with cleavage at few dendritic regions. Impact testing was carried out at room temperature and 233 K (−40 °C). Impact toughness was low owing to asymmetric plastic zone. Deformation was one-sided and crack moved through ferrite. Weld cracking did not show any effect over tensile crack propagation.

As a substitute of conventional fusion welding discussed above, friction stir welding (FSW) of ferritic and austenitic stainless steel were also attempted for fabricating other structural components.^[21] FSW of austenitic steel was rather simple as it did not undergo any phase transformation during welding. At weld nugget due to dynamic recrystallization grain refinement occurred. In case of C–Mn steel, the process became complex. Depending on peak temperature and heat input stirring zone, thermomechanically processed zone and heat-affected zone of the specimen experienced different thermal states. Based on chemical composition, carbon equivalent, and the heat treatment condition various phase transformations occurred at different regions. Failure and Joint efficiency under tensile loading depended on final microstructure of the weakest link within weld.

From above discussion, it is evident that information is available for dissimilar metal weld consisting of ferritic and austenitic steel where main focus was to explore microstructural features accompanied by evaluation of mechanical properties. Apart from cost and time of fabrication of such joints, heat treatment played a vital role in altering the property of joint along with its microstructure. Information related to effect of stress

relief annealing/post weld heat treatment on microstructure and mechanical properties is scanty in this respect. Even, during illustration it was not clearly mentioned whether post-weld heat treatment has been carried out or not. In the present endeavor, attempts have been made to study the effect of stress relief annealing on the microstructural features and mechanical properties for joints between LAS and austenitic stainless steel. Different buttering materials were used and a set of weld from each group was heat treated for stress relieving. Ultimate aim was to investigate the feasibility of heat treatment and finding out better welding consumable to obtain adequate reproducible weld efficiency, desired for nuclear power plant application.

II. EXPERIMENTAL

Base materials were SA508 Gr.3 Cl.1 low alloy steel (LAS) and SA312-type 304LN austenitic stainless steel (304LN SS). Chemical composition of base materials and welding consumables is presented in Table I. Bulk chemical composition of steel and stainless steel was determined by spark emission spectrometry. In this technique, rectangular block of $\sim 20 \text{ mm}^2$ cross section was taken, polished, cleaned in acetone, and exposed to electrode for creating spark. Readings were directly obtained over viewing screen. In case of Ni-base alloys, turnings were taken and dissolved in acidic solution. Bulk composition of the alloy was determined by inductively coupled plasma spectrometer using that solution. In all four alloys, the concentration of carbon, sulfur, and nitrogen was evaluated by LECO gas analyser using fine turnings.

Four different DMW joints were prepared and their details are furnished in Table II. Stress relief annealing for one set of joints was carried out at $\sim 923 \text{ K}$ ($650 \text{ }^\circ\text{C}$) for 90 minutes. Schematic of weld joint is shown in Figure 1(a). Thickness of virgin carbon and stainless steel was $22 \pm 1 \text{ mm}$. From welded joints, sampling has been done along transverse section and prepared by

conventional metallographic technique.^[22] Etching was done for LAS side with Nital and for remaining part with Glycergia. Specimens were initially examined in optical microscope to identify gross change in microstructure. Region close to fusion boundary was studied in scanning electron microscope to identify characteristics of different regions. During examination of samples, the area was scanned from top to root of weld to explore variation in microstructure. Representative images were taken from the mid-section of thickness direction. Quantification of microstructural features was performed in image analysis software.

X-ray diffraction experiment was carried out near fusion boundary-1 (FB-1, *i.e.*, between LAS–buttering material) to identify phases formed due to diffusion. Parameters during investigation were 40 kV to 40 mA with two theta angular rotational range of 30 to 100 deg for specimen. Step size was 0.04 deg ($= 2\theta/s$) at the time of experimentation. $\text{Cu K}\alpha$ was used as source with wavelength $\sim 1.542 \text{ \AA}$. Semi-conductor detector was ‘LynxEye.’ Rectangular slit with dimension 8 mm length \times 1.5 mm width was used to control the incidental beam dimension. Sampling procedure for the same has been illustrated in Figure 1(c). Initially the whole assembly was taken, polished metallographically over transverse section, and etched with Nital to identify different regions. FB-1 was clearly visible. Then using EDM, material to the left of Layer-1 parallel to FB-1 was removed and once again the fresh surface perpendicular to transverse section was polished and cleaned. X-ray diffraction was been done over it and characteristic peaks were identified. In the next step, material to the left of Layer-2 was removed and same steps were carried out for X-ray diffraction experiment. In that way, after crossing FB-1 (the dark firm line), we reached extreme right border as shown (dotted dark line). In all steps, the X-ray peaks were identified and thus the phases across the fusion boundary were confirmed.

Microhardness was determined across FB-1 of weldment. Readings were taken as per ASTM E384 standard

Table I. Chemical Composition of Base Metals and Welding Consumables

| Alloy | Concentration of Alloying Elements (wt pct) | | | | | | | | | | | | |
|-------|---|-----|------|-------|-------|------|------|------|------|------|-----|-----|------|
| | C | Mn | P | S | Si | Ni | Cr | Mo | Cu | Al | N | Nb | Fe |
| LAS | 0.20 | 1.2 | 0.01 | 0.001 | 0.001 | 0.80 | 0.20 | 0.50 | 0.03 | 0.04 | — | — | bal |
| 304LN | 0.03 | 2.0 | 0.05 | 0.03 | 1.0 | 8.0 | 18.0 | — | — | — | 0.1 | — | bal |
| IN182 | 0.10 | 5.0 | 0.03 | 0.02 | 1.0 | bal | 13.0 | — | 0.5 | — | — | 1.0 | 10.0 |
| IN82 | 0.10 | 3.2 | 0.03 | 0.01 | 0.4 | bal | 19.0 | — | — | — | — | 2.5 | 2.0 |

Table II. Welding Technique and Sample Identification

| Sample | Welding Consumable | Buttering | Welding Process | Stress Relief Annealing Temperature |
|---------|--------------------|-----------|-----------------|--|
| IN82W | IN82 | GTAW | GTAW | no annealing |
| IN82HT | IN82 | GTAW | GTAW | yes, $\sim 923 \text{ K}$ ($650 \text{ }^\circ\text{C}$) |
| IN182W | IN182 | SMAW | SMAW | no annealing |
| IN182HT | IN182 | SMAW | SMAW | yes, $\sim 923 \text{ K}$ ($650 \text{ }^\circ\text{C}$) |

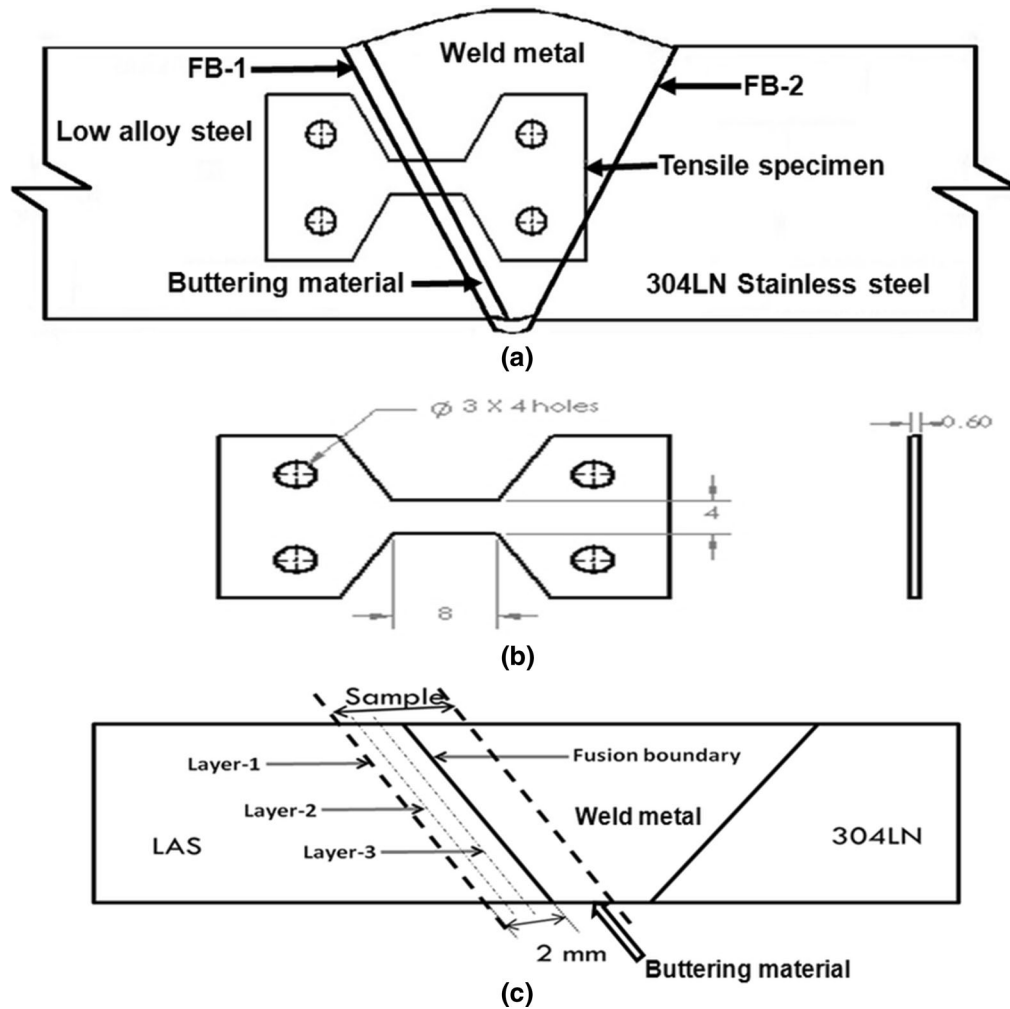


Fig. 1—Schematic diagram of transverse section of dissimilar metal weld (a) sampling location of tensile specimen, (b) enlarged view of tensile sample, and (c) sampling technique for XRD specimen (not to scale).

at an interval of ~1.0 mm using 50-g-force load and 15 seconds dwelling time.

In situ tensile testing was done in scanning electron microscope. Miniature samples were prepared keeping FB-1 nearly at center of gage length (Figure 1(b)). Experiments were carried out on tensile stage with 2 kN load cell, attached to SEM. Before testing, both surfaces of specimen were made flat and scratch-free with mirror finish. At each joining parameter, a minimum of three samples were tested to confirm its repeatability. Cross-head speed during tensile testing was ~0.05 mm/min, and data acquisition rate was ~500/s. Images were recorded during testing to study deformation characteristics as well as fracture.

III. RESULTS

Microstructure of as-received low alloy steel consisted of tempered martensite. 304LN SS exhibited existence of polygonal austenite grains with annealing twins. Microstructure of LAS after fabrication could be divided into few zones like Zone-2 and Zone-3. These

were developed owing to welding/welding followed by stress relief annealing (Figure 2). Here, Zone-1 corresponded to unaltered base metal (not shown in images). Zone-2 presented polygonal ferrite grains with pearlite. Zone-3 which was adjacent to FB-1, revealed coarse ferrite grains with dispersion of carbides.

Two different boundaries were identified at BCC-FCC interface within buttering material (Figure 3). One was nearly perpendicular to FB-1 and known as Type-I boundary. The other one was parallel to FB-1, termed as Type-II boundary. Type-I boundary appeared as an effect of columnar growth at interface and were aligned perpendicular to fusion boundary. Type-II boundary was a typical grain boundary that was oriented approximately parallel to fusion boundary, located at a very short distance within fusion zone.^[23] Narrow crisscross band of a newly formed phase was found close to FB-1 and was well within Type-II boundary throughout length (Figure 4). This new phase at later stage was identified in X-ray diffraction. Distance of Type-II boundary from FB-1 as well as thickness of newly formed phase was variable. Both of them were discontinuous in nature. Type-I boundary

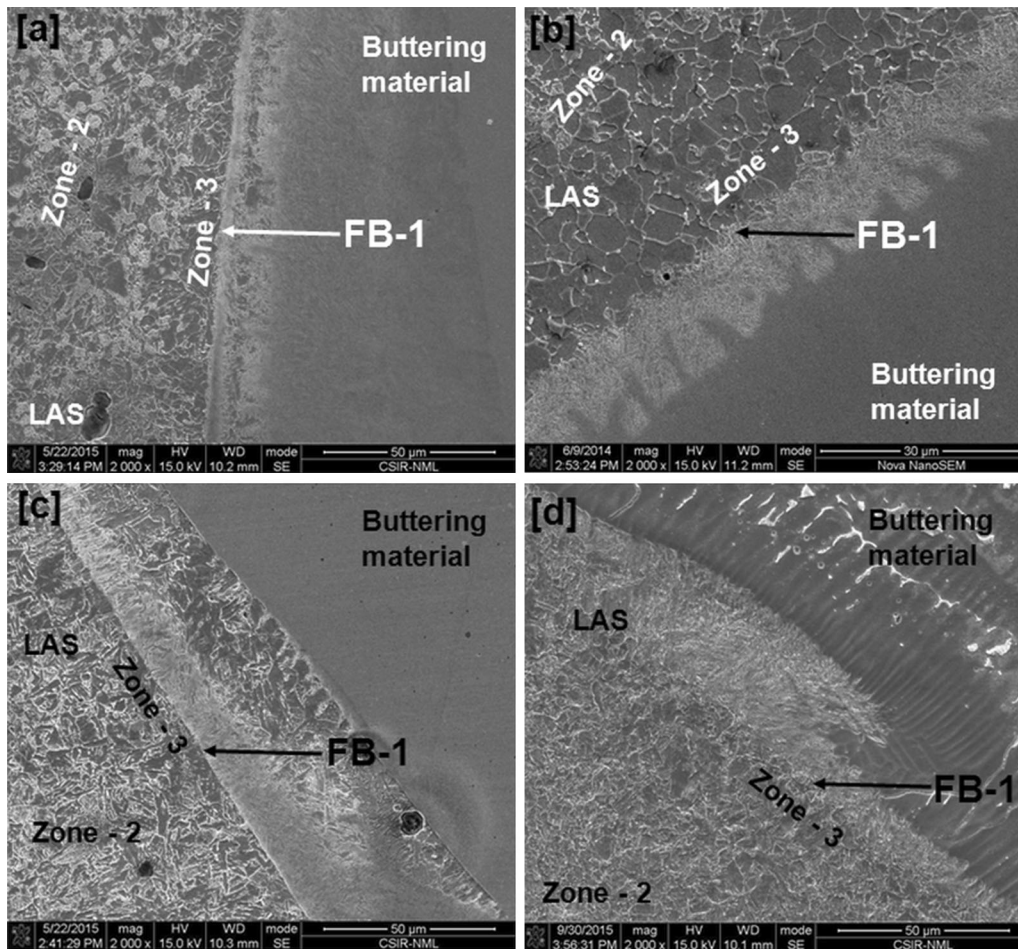


Fig. 2—Images close to LAS–buttering material interface revealing different zones in LAS side (a) IN82W, (b) IN82HT, (c) IN182W, and (d) IN182HT (deeply shaded spots were etch pits).

also did not maintain homogeneity in terms of its location with respect to FB-1.

Figures 5 and 6, revealed solidification microstructure of layerwise deposited buttering material.^[11] Close to FB-1 (Figure 5), the substructure was cellular with evenly spaced fishing net along with solidification boundaries. Predominantly Austenitic/Ferritic (AF) and occasionally Ferritic/Austenitic (FA) modes of solidification were observed near FB-1. Away from fusion boundary (Figure 6), solidification occurred in austenitic phase with extensive grain boundary migration as a result of coalition of subgrains.^[24] In present investigation, both buttering material and weld metal were of same composition, hence no sharp unmixed zone was formed between them (Figure 7). The mismatch as revealed in images was due to change in orientation of dendritic arms during solidification. Figure 8 indicated area around FB-2, formed between weld metal and austenitic stainless steel. A narrow discontinuous region containing spheroids/plates was found and perhaps was the outcome of partial melting followed by solidification of weld metal.^[17] Quantitative microstructural information of different characteristics has been collated in Table III.

Microhardness profiles across FB-1 for all welds are given in Figure 9. Close to FB-1, all profiles exhibited a peak of ~330 to 340 VHN. Immediately before and after peak hardness, in LAS and buttering material, respectively, the profile exhibited sharp fall. Hardness in those regions reached minimum level. The extent of minima was lowest within buttering material than that of LAS side. Marked difference was observed regarding the location of peak. In as-welded condition, the peak was close to LAS side (Figures 9(a) and (c)). After heat-treatment, it was shifted toward buttering material (Figures 9(b) and (d)).

The phases near FB-1 were confirmed through X-ray diffraction technique (Figure 10). Apart from bcc α -Fe of LAS and γ phase of Ni alloys, the newly formed phase was confirmed as martensite adjacent to FB-1. The phase fraction of martensite was small with respect to bulk and was endorsed by tiny spikes in characteristic spectrum. Apart from them, other complex alloy carbide/iron carbide might be present adjacent to interface, but not identified in present investigation perhaps because of their small volume fraction/nano scale size.^[8,25]

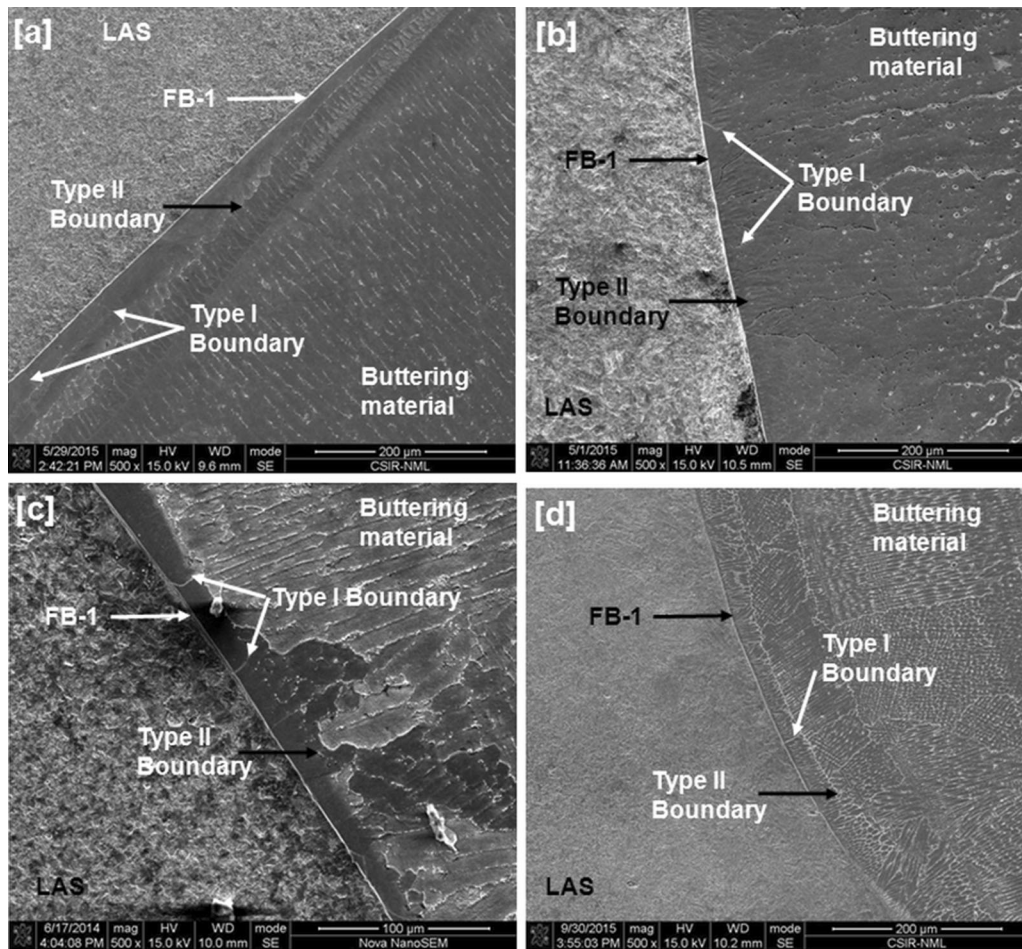


Fig. 3—SEM micrographs across LAS–buttering material fusion boundary exhibiting different microstructural heterogeneities (a) IN82W, (b) IN82HT, (c) IN182W, and (d) IN182HT (deeply shaded spots were etch pits).

Engineering stress–strain plots as shown in Figures 11(d), 12(d), 13(d), and 14(d) exhibited the variation of mechanical properties of different joints. Transition joints exhibited highest strength in welded condition (Table IV). Stress relief annealing reduced bond strength with marginal improvement in ductility. In welded condition, IN82W demonstrated highest tensile strength. Heat treatment decreased strength to the tune of 7 to 12 pct for same joint. Similar trend was observed for joints fabricated with IN182 buttering material; however, in heat-treated condition, the reduction was less (~2 to 5 pct). Overall elongation of weld fabricated with IN82 was better than joints produced with IN182. During deformation, SEM–SE images were captured to observe structural changes. Until yield point no significant changes were found. Shear bands appeared when samples started undergoing uniform plastic deformation. They were characterized by massive collective dislocation activity in a narrow local deformation zone while the abutting matrix underwent comparably homogeneous flow.^[26] Failure was through microvoid coalescence exhibiting characteristics of ductile dimple rupture. In all cases, failure was within buttering material; however a difference was observed for as-welded samples with respect to welded-stress

relief-annealed samples. In the annealed samples, crack was initiated away from FB-1 and propagated nearly parallel to fusion boundary (~2 to 2.5 mm). In welded samples, the crack initiation was from FB-1 making an angle of ~55 to 65 deg, propagated in zigzag fashion through buttering material.

IV. DISCUSSION

The transverse section of welded joint displayed a complex microstructure in which different heterogeneities were present. Zone-2 and 3 within LAS could be considered together as heat-affected zone.^[27] At Zone-3, material reached temperature as high as melting point of the alloy during welding. When it cooled down through austenitic region, pro-eutectoid ferrite and pearlite formation took place.^[27] Occurrence of refined ferrite–pearlite structure was also indicated for laser beam welded similar grade St37 and 52 joints.^[19] Due to concentration gradient of chemical species across fusion boundary, atomic migration of major alloying elements occurred during welding. Carbon and iron migrated from LAS side to buttering material. Similarly, nickel and chromium diffused from buttering material to low

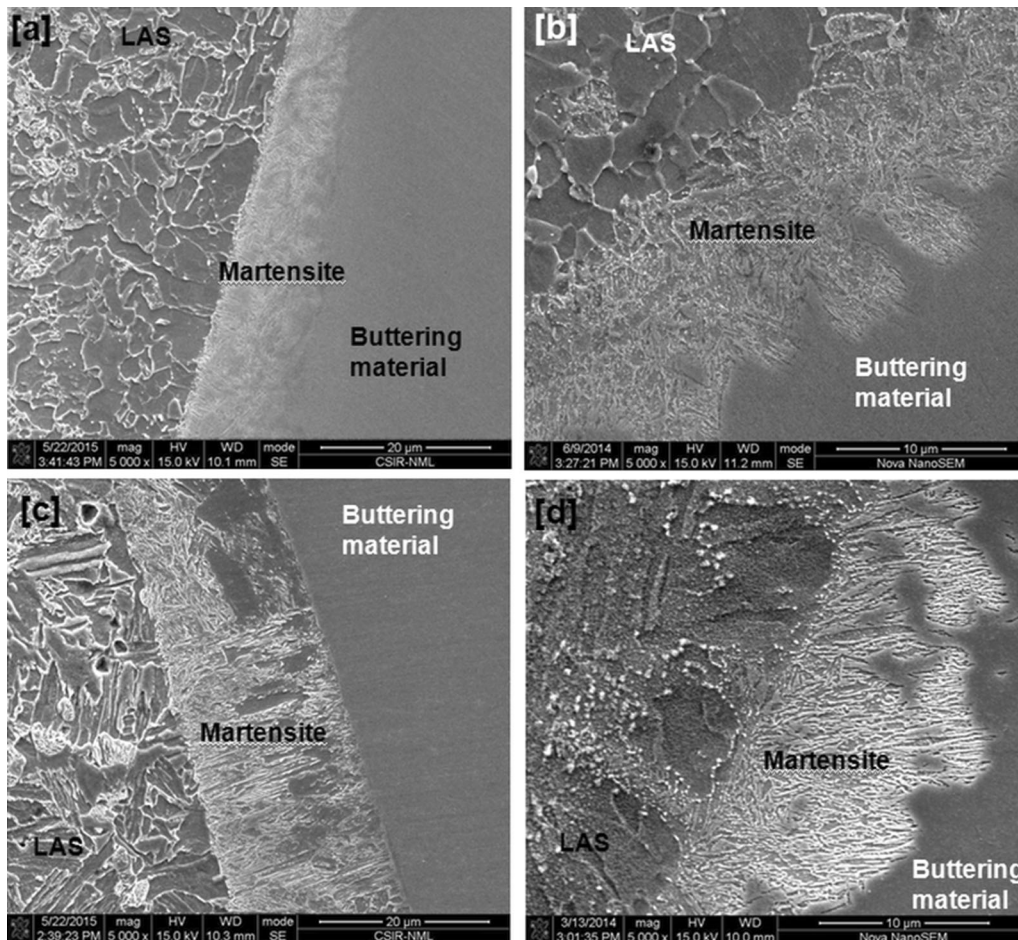


Fig. 4—Lath martensite near fusion boundary between LAS–buttering material (a) IN82W, (b) IN82HT, (c) IN182W, and (d) IN182HT (deeply shaded spots were etch pits).

alloy steel. Among all these diffusing species, carbon was the fastest.^[3] Carbon diffusion from area adjacent to FB-1 created a depleted region and reduced iron carbide fraction. Grain boundary pinning owing to presence of carbides became less effective.^[6] Grain size increment thus resulted in coarse ferritic grain in Zone-3. In Zone-2, the maximum temperature was within inter-critical region.^[27] Tempered martensitic structure of low alloy steel transformed into stable ferrite–pearlite/cementite combination. Mixture of two phases, *i.e.*, ferrite and cementite restricted the grain growth in this region.^[27] Therefore, Zone-2 consisted of fine grain ferritic structure with clustered cementite islands/pearlite. When stress relief annealing was carried out, atomic migration of carbon and other elements occurred across FB-1. Moreover, for left over part of LAS, metastable-tempered martensitic structure transformed to stable ferrite–cementite/pearlite combination. In synergistic effect, the total width of Zone-2 and 3 for welded–annealed specimens was increased with respect to welded specimen. The variation in width of different zones is given in Table IV, which clearly indicates the effect of annealing treatment of welded specimens. It has been found that, average width of Zone-3 was more for IN182W with respect to IN82W. Buttering with IN182

was carried out with SMAW and IN82 was done by GTAW. Heat input in case of the former was higher than the latter.^[25]

The presence of Type-I and Type-II boundaries was observed close to FB-1 in buttering material side. Nelson *et al.*^[29] explained that shortly after solidification, the fusion boundary, formerly a BCC–FCC interface that suppressed normal epitaxial growth became an FCC–FCC interface. This could be considered as mobile high energy boundary. The boundary migrated into face-centered cubic nickel base buttering material. Migration was controlled by the temperature gradient.^[26,28] It was then ceased in that place as the weld metal cooled. Type-II boundary formation was followed by the transformation of carbon steel substrate to a mixture of ferrite, cementite, and martensite.^[29] Since, the heat input was higher for SMAW than GTAW, the boundary migration was faster for IN182W than IN82W. The same characteristic was depicted in Table III by higher average distance of Type-II boundary from FB-1 in case of former with respect to later. Elemental spot analysis suggested that Type-I and Type-II boundaries were chemically similar considering their bulk composition (Figure 15(c) – spot 1, 3, 5, and 6; Figure 15(d) – spot 1 and 4). Slight enrichment in

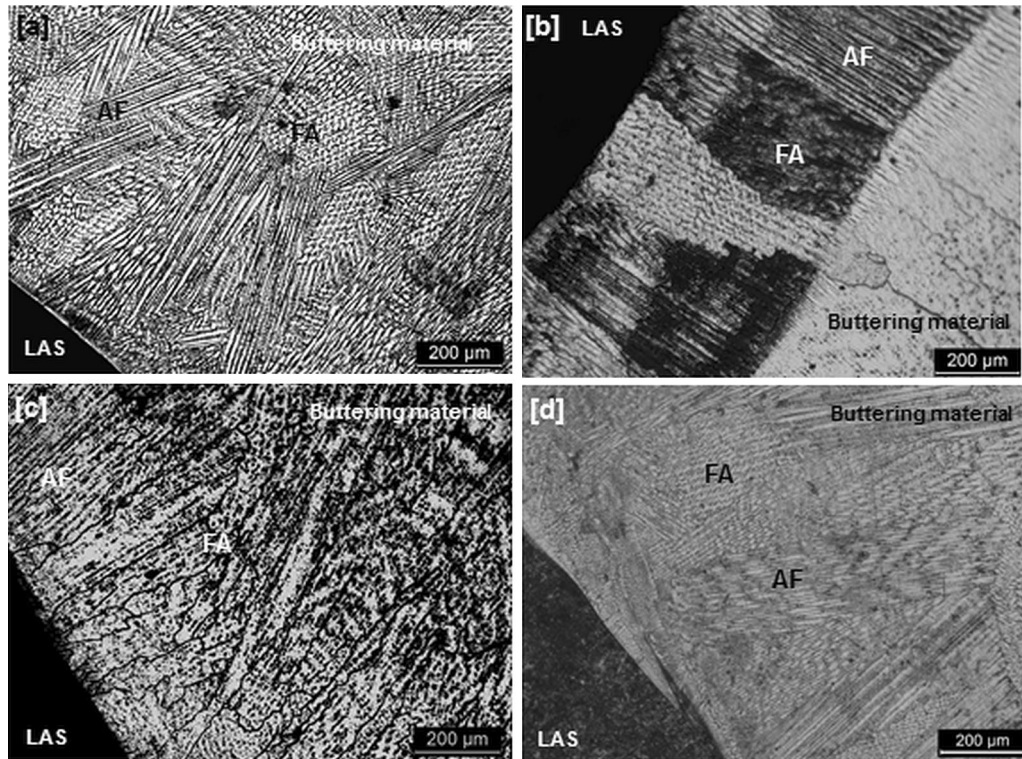


Fig. 5—Solidification microstructure of buttering material close to FB-1 (a) IN82W, (b) IN82HT, (c) IN182W, and (d) IN182HT.

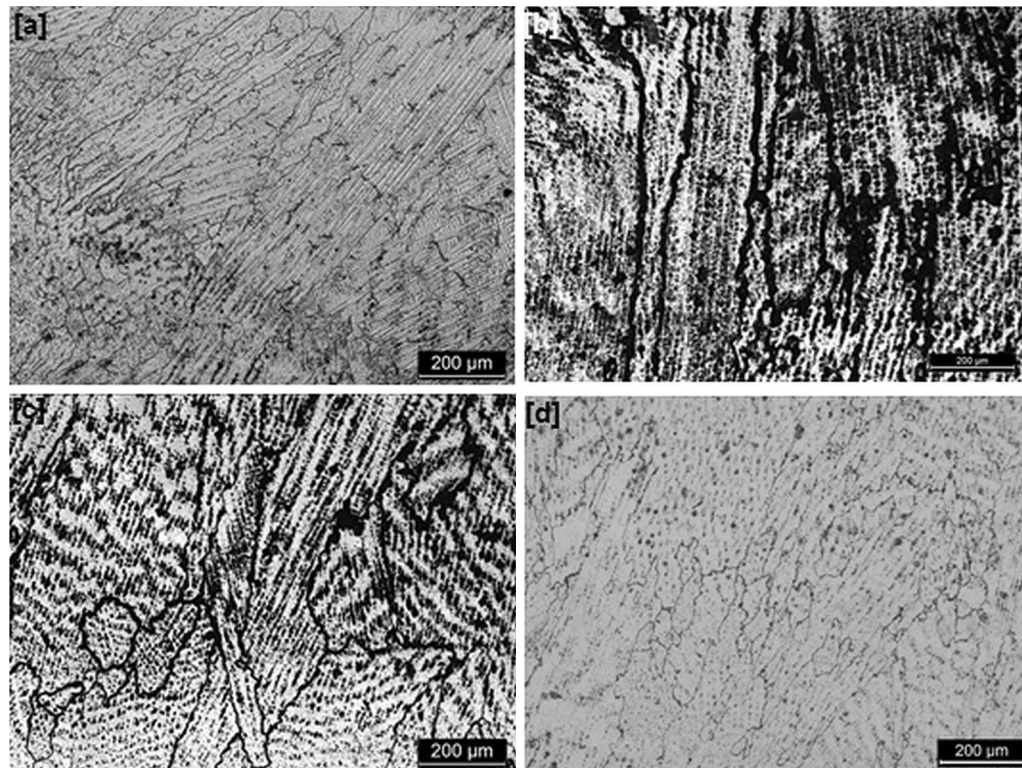


Fig. 6—Solidification microstructure of buttering material away from FB-1 (a) IN82W, (b) IN82HT, (c) IN182W, and (d) IN182HT.

carbon and iron was observed in those regions with respect to IN182 bulk composition. This happened owing to atomic migration of carbon and iron from low

alloy steel to buttering material during welding. In few locations, niobium-rich complex precipitates were found (Figures 15(a) and (b)). These precipitates restricted the

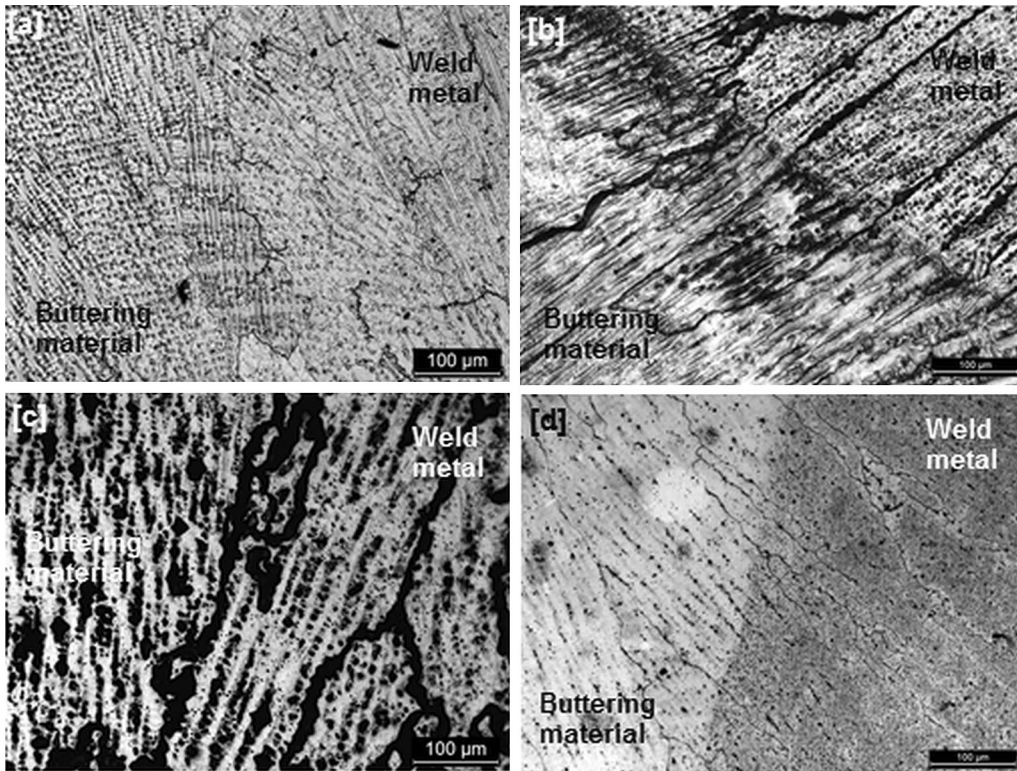


Fig. 7—Buttering material–weld metal interface (a) IN82W, (b) IN82HT, (c) IN182W, and (d) IN182HT.

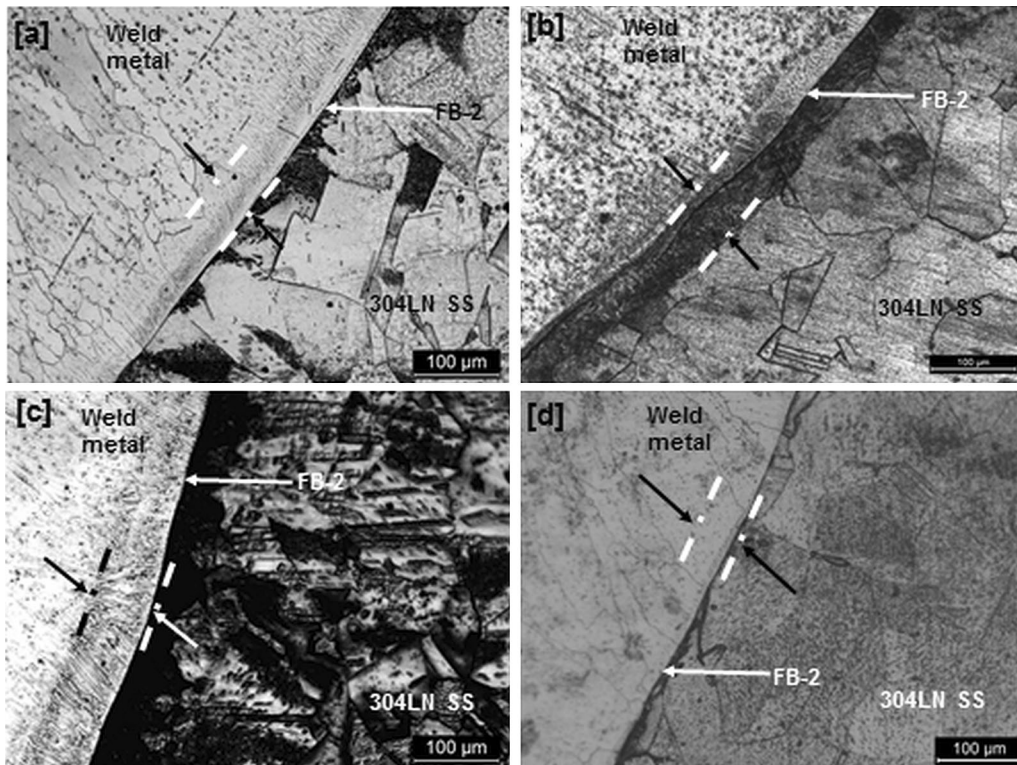


Fig. 8—Fusion boundary-2 between weld metal–304LN SS exhibiting sharp interface (a) IN82W, (b) IN82HT, (c) IN182W, and (d) IN182HT.

Table III. Quantitative Analysis of Microstructural Features

| Sample ID | Thickness of Martensite Layer (μm) | | Distance of Type-II Boundary from FB-1 (μm) | | Width of Fine Grain HAZ in LAS (zone-2, μm) | | Width of Coarse Grain HAZ in LAS (Zone-3, μm) | |
|-----------|---|------|--|------|---|------|---|-----|
| | Max | Min | Max | Min | Max | Min | Max | Min |
| IN82W | 34.0 | 10.6 | 30.0 | 10.0 | 1103 | 909 | 441 | 166 |
| IN82HT | 13.8 | 7.5 | 29.2 | 12.5 | 1681 | 836 | 454 | 308 |
| IN182W | 19.8 | 13.7 | 40.7 | 12.3 | 1608 | 1055 | 625 | 254 |
| IN182HT | 11.1 | 7.8 | 42.6 | 7.4 | 1744 | 1029 | 655 | 236 |

boundary movement. For this reason, not much difference was observed regarding the location of these boundaries between welded and welded-stress relief-annealed specimens (Table III).

Mode of solidification was changed from cellular to dendritic due to the presence of Niobium in Inconel filler material that has intense tendency to promote constitutional under-cooling.^[24] The equilibrium distribution coefficient of Nb was minimum. Therefore, it was easily redistributed within interdendritic regions during solidification and produced Nb-enriched carbides.^[24] FB-2 was developed between weld metal and 304LN SS. Considering bulk composition, Ni alloy was completely different with respect to 304LN SS. An unmixed zone thus appeared with sharp demarcation line (Figure 8). Adjacent to this interface, 304LN SS exhibited grain coarsening because of temperature rise during welding. Severe grain growth ($\sim 85 \mu\text{m}$) occurred for matrix grains of 304LN SS with respect to base material ($\sim 55 \mu\text{m}$) for welded specimens.

Microhardness distribution across FB-1 exhibited a near-symmetric profile. In as-welded specimens the peak was observed close to FB-1 (Figures 9(a) and (c)). Peak hardness was a synergistic effect of two phenomena. As mentioned before, welding was followed by temperature drop producing thin martensite layer adjacent to FB-1 with high hardness. At the same time, Cr and Nb were two strong carbide formers in Ni alloys and produced tiny alloy carbides in LAS with available carbon after migrating through FB-1.^[3] These complex carbides also contributed significantly in enhancing the microhardness. After heat treatment though peak value of hardness did not change significantly, yet the peak shifted away from FB-1 toward buttering material (Figures 9(b) and (d)). Stress relief annealing at $\sim 923 \text{ K}$ ($650 \text{ }^\circ\text{C}$) temperature, which was lower than peak temperature during welding, did not change the nature of carbide, except coarsening to a small extent. Increment in size reduced strengthening effect. Peak was shifted because of two reasons. Previously formed martensite was tempered during heat treatment and region contained fine dispersion of iron carbide. Reduction in martensitic layer thickness as depicted in Table IV envisaged the phenomenon. Secondly, stress relief annealing caused further carbon migration into buttering material and fresh martensite formed adjacent to tempered martensitic region.^[6] The peak hardness in welded specimen close to FB-1 was also reported by Seifert *et al.*^[8] for DMW between SA508 and IN182. They inferred that

increased hardness was owing to presence of carbides and/or martensite-like microstructure. Dissimilar weld consisting of St37-austenitic stainless steel reported the peak hardness of ~ 380 to 400 Hv within weld zone due to the presence of hard constituents like bainite and/or martensite.^[19] Dissimilar joint of St52-austenitic stainless steel exhibited hardness peak ($\sim 425 \text{ Hv}$) within ferrite and it was higher than the hardness of weld metal ($\sim 400 \text{ Hv}$).^[19] High hardness in narrow HAZ was attributed to the presence of martensite. The variation in location and value of peak hardness in present investigation with respect to the findings as stated above may be because of difference in welding procedure and consumables. The immediate drop in microhardness in LAS side was attributed to the presence heat-affected zone.^[3,4,17] Similarly, within buttering material adjacent to FB-1, the solidification microstructure also exhibited a drop in microhardness of the alloy. However, average microhardness of this region was higher than virgin buttering material hardness owing to solid solution strengthening caused by migration of Fe and C during processing.^[4]

In as-welded condition greater ultimate tensile strength of IN82W with respect to IN182W might be attributed to the inherent higher strength of former with respect to later (Table IV). Shear bands appeared in buttering material for both welds after yield point. This became common characteristics of deformation for FCC material.^[30] No deformation was observed in LAS side, as this alloy was relatively stronger than buttering material. Region close to FB-1 showed high hardness and acted as stress concentration site. Crack was initiated from that location at a certain stage of deformation. Failure path was completely through softest region of weld, *i.e.*, buttering material in zigzag fashion (Figures 11(b), 12(b), 13(b)). Nature of crack propagation was governed by orientation of dendritic arms during solidification and the orientation of shear bands.^[4] Shear bands of same orientation formed packet and there are several such packets within buttering material. Crack movement also controlled by the boundary of such packets.

Crack initiation in stress relief-annealed samples was away from FB-1 (Figures 12(b) and 14(b)). This might be corresponded to the shift in peak microhardness in annealed samples. In these specimens it was expected that dendritic structure disappeared partially/completely. In that case, adjacent to FB-1, a composite structure emerged consisting of tempered martensite/

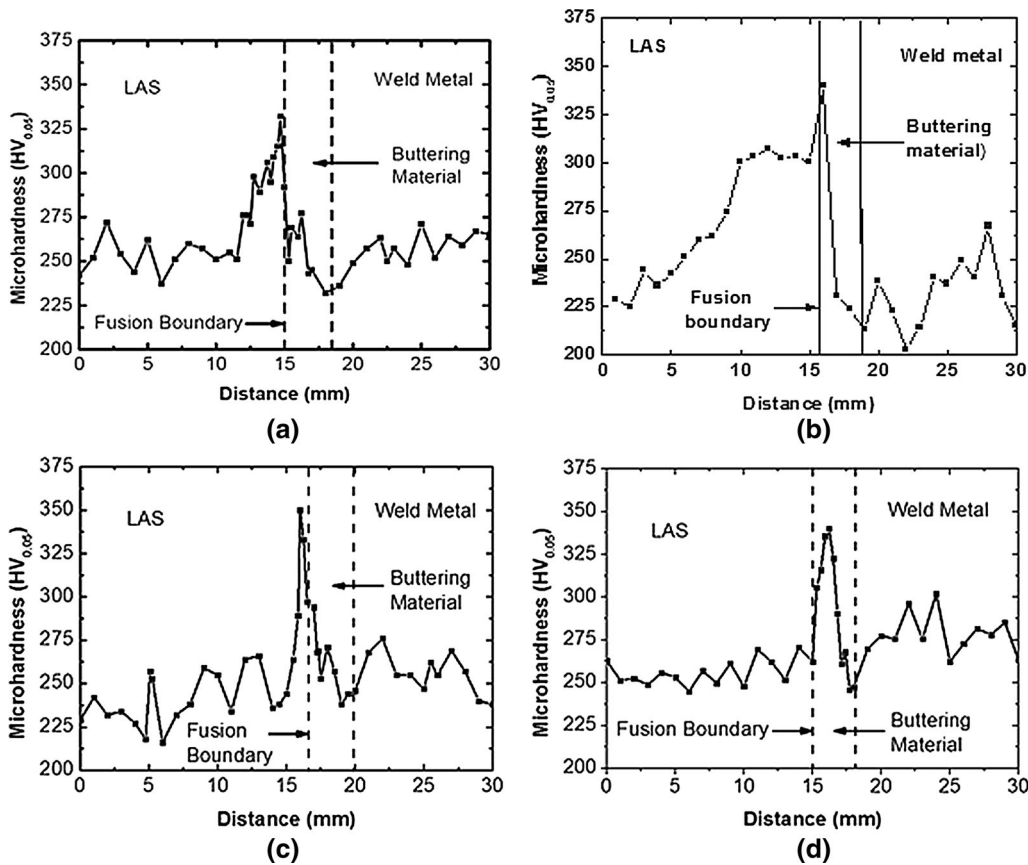


Fig. 9—Microhardness profile across FB-1 of welds (a) IN82W, (b) IN82HT, (c) IN182W, and (d) IN182HT.

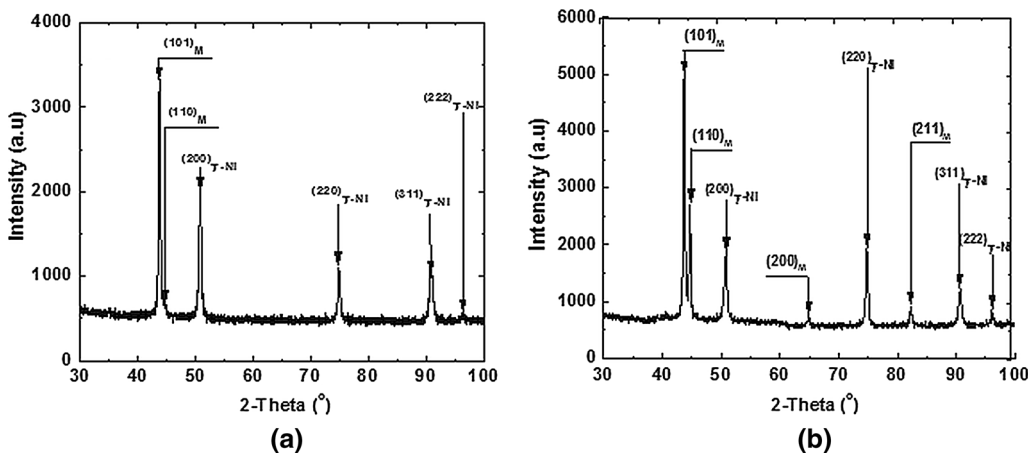


Fig. 10—X-ray diffraction study near FB-1 of (a) IN82HT and (b) IN182HT.

freshly formed martensite along with Type-I and II boundaries. Therefore, a virtual boundary was created between hard and soft phase, which was nearly parallel to fusion boundary. Moreover, stress relief annealing resulted in re-orientation of grain boundary and collection of planar defects in a particular orientation.^[26] Therefore, crack formed at the edge and moved along this virtual boundary. At the time of failure, it appeared as nearly parallel to FB-1. Orientation of shear bands in this case also endorsed the existence of such virtual

boundary (arrow in Figures 12(b), (c) and 14(b), (c)). For these samples, only two sets of shear bands were found nearly perpendicular to FB-1 generating mid-rib type of appearance (Figures 12(b) and 14(b)).

Above all, annealing released the stress that was developed during welding of dissimilar material due to difference in thermal expansion coefficient between them.^[5] This was responsible for softening of the alloy and overall strength of the joint was reduced with a marginal increment in breaking strain. In all welds though

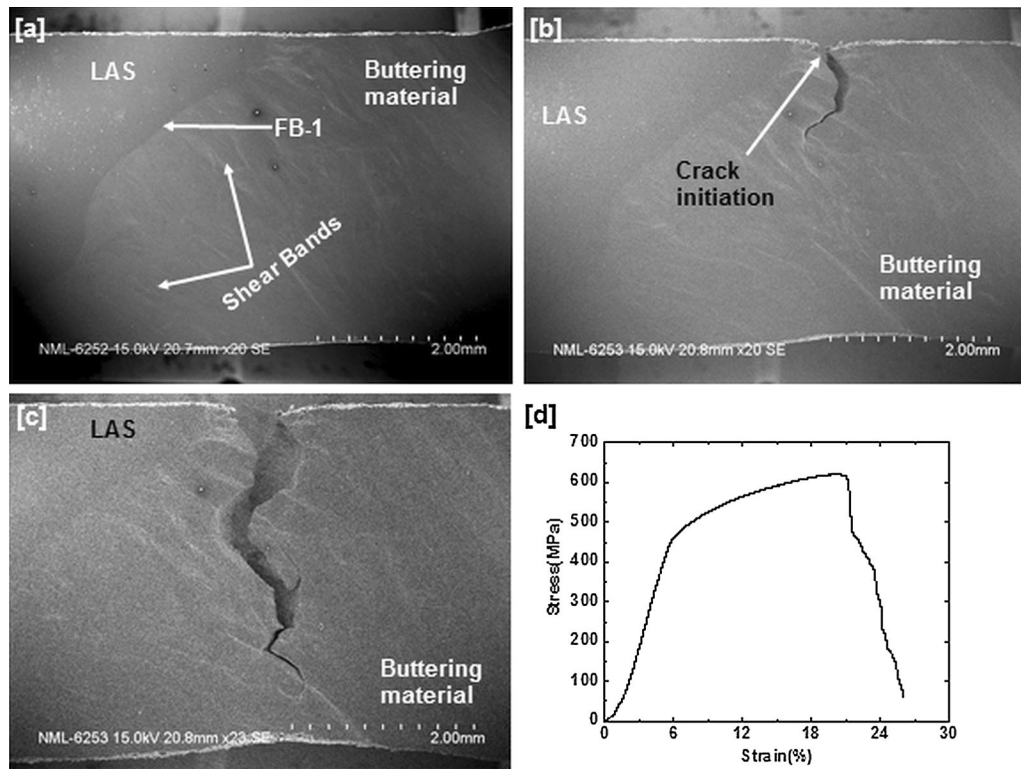


Fig. 11—SEM-SE images during tensile test of IN82W (a) appearance of shear bands, (b) crack initiation, (c) crack propagation, and (d) engineering stress-strain diagram of one specimen.

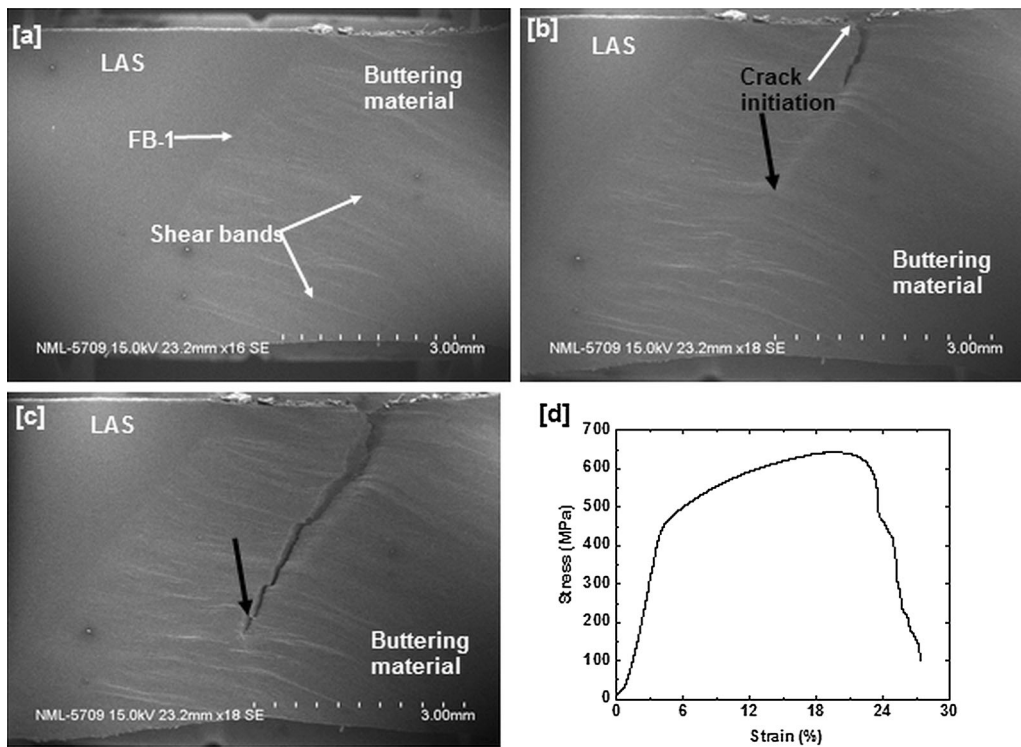


Fig. 12—SEM-SE images during tensile testing of IN82HT sample (a) shear bands, (b) crack initiation, (c) crack propagation, and (d) engineering stress-strain curve of one sample.

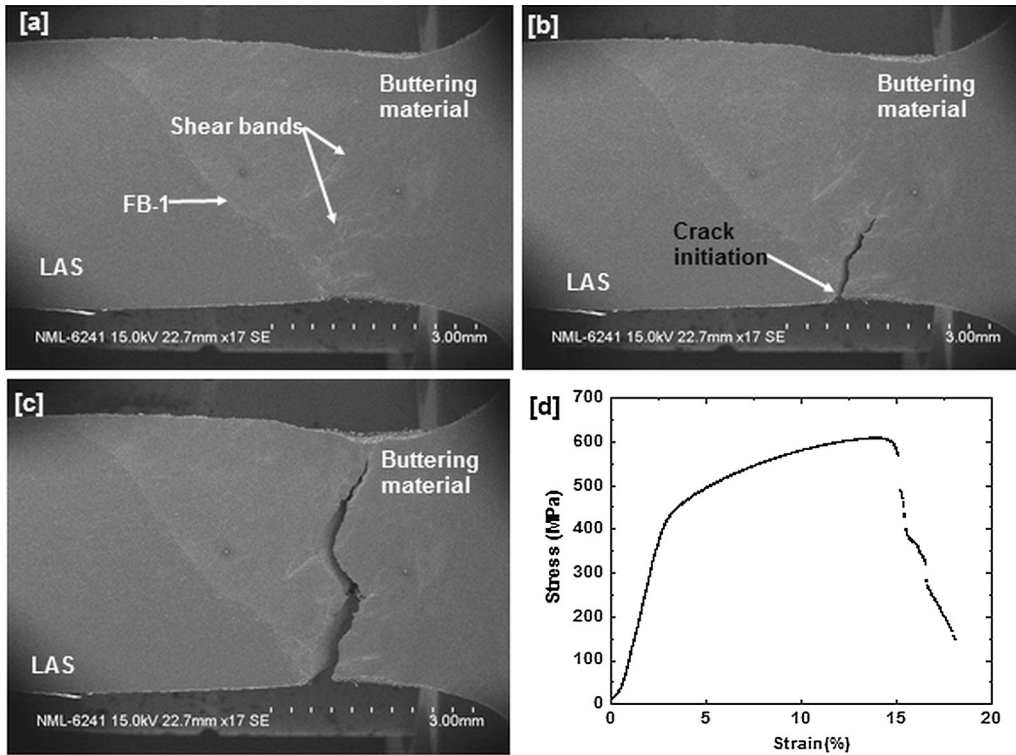


Fig. 13—SEM-SE images during tensile testing of IN182W (a) formation of shear bands, (b) crack initiation, (c) crack propagation, and (d) engineering stress–strain diagram of one of the samples.

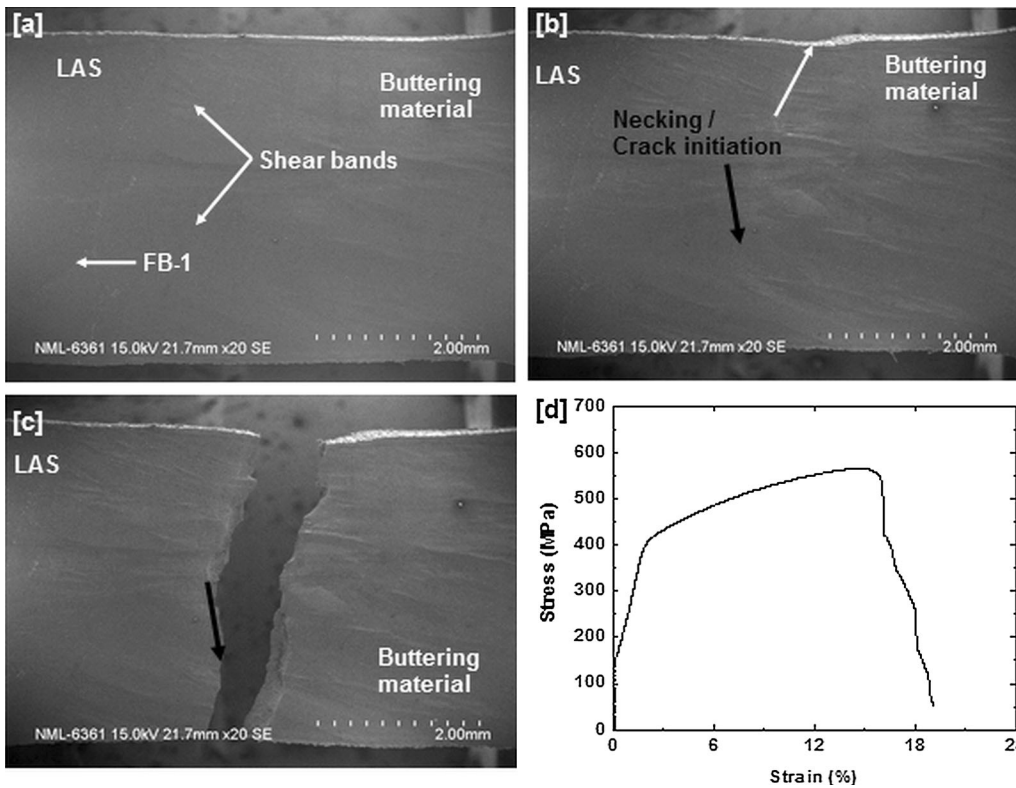


Fig. 14—SEM-SE images during tensile testing of IN182HT sample (a) shear bands, (b) necking/crack initiation, (c) crack propagation, and (d) engineering stress–strain plot of one specimen.

Table IV. Tensile Properties of Welds Across FB-1 at Room Temperature

| Sample ID | Yield Strength (MPa) | Ultimate Tensile Strength (MPa) | Breaking Strain (pct) |
|---------------|----------------------|---------------------------------|-----------------------|
| IN82W | 458 ± 2 | 625 ± 5 | 19.2 ± 0.4 |
| IN82HT | 392 ± 11 | 584 ± 12 | 20 ± 0.5 |
| IN182W | 411 ± 10 | 594 ± 10 | 16 ± 1.5 |
| IN182HT | 379 ± 3 | 583 ± 12 | 17.7 ± 1.8 |
| Virgin IN 82 | ~360 | ~590 | ~38 ^[29] |
| Virgin IN 182 | ~310 | ~552 | ~30 ^[30] |

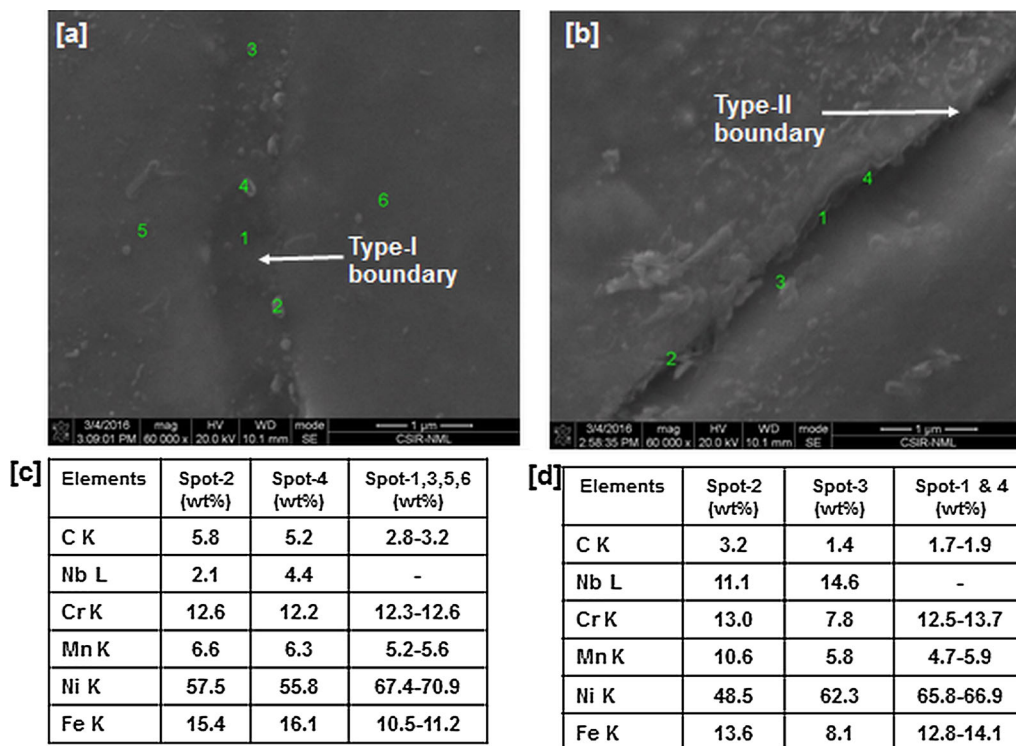


Fig. 15—SEM-SE images of IN182W sample near FB-1 (a) complex carbide dispersion within Type-I boundary, (b) Nb-Cr-rich carbide islands in Type-II boundary, and (c), (d) semi-quantitative spot analysis using EDS for selective regions.

failure was through buttering material yet the strength level showed little higher value with respect to virgin buttering alloy perhaps due to solid solution strengthening of the same by chemical species migrated from low alloy steel side. Strengthening, on the other hand, abated ductility of weld with respect to virgin buttering alloy.

Jang *et al.* evaluated the tensile strength of welded joint consisting of carbon steel and stainless steel with Ni-base buttering material.^[16] They observed variations in UTS and YS of 500 to 550 MPa and 350 to 400 MPa, respectively. It was concluded that grain coarsening, sample thickness, and sampling location were main influential factors. Different austenitic weld metals were used in fabricating joints between Alloy 800 and stainless steel.^[2] In this respect, IN82 provided maximum strength and joints produced with 16-8-2 stainless steel weld metal exhibited minimal joint strength. It was also observed, that welded joints produced with austenitic stainless steel became prone to failure along fusion line. Similar type of attempt was made for joining austenitic stainless steel and IN657.^[31] In that case, four

welding metals such as IN82, IN617, IN A, and 310 SS were used. The study revealed that IN A alloy imparted maximum weld strength with adequate ductility, IN82 reduced the weld strength to the maximum extent and IN617 decreased the breaking strain to lowest value. Use of IN82 and 182 for welding of same base material showed parent material failure during tensile testing. Ductility was substantially improved for welded joint containing Ni alloy weld metal than that of containing austenitic stainless steel. In a different endeavor, austenitic stainless steel was welded with 0.17C-1.4Mn carbon steel through 85Ni-19.2Cr stainless steel weld metal.^[1] Failure took place from interface between stainless steel and weld metal during tensile testing. This fact was attributed to low initial residual stress of austenitic stainless steel with an ability to withstand against maximum plastic stain during testing. Attempts were made to evaluate the strength of laser beam-welded carbon and stainless steel.^[19] Tensile testing of microspecimen, where interface was at the center of gage length, reported failure from ferritic steel side.

Maximum strength was ~540 MPa and 420 MPa for St52-austenitic stainless steel and St37-austenitic stainless steel, respectively. Both these values were lower than UTS of any specimen in present endeavor. Micro-tensile specimens were obtained from different regions of weld to determine local mechanical properties. St37-stainless steel joint and St52-stainless steel joint in that case exhibited highest strength at weld region owing to the presence of hard microstructural constituent. Strength of HAZ of ferritic steel was between virgin ferritic steel and weld metal. HAZ of austenitic steel did not reveal any significant change.

As stated initially, failure of this type of DMW mainly occurred from/along FB-1.^[6,12] Perhaps all structural heterogeneities like martensite layer, Type-I and II boundaries synergistically contributed in it. The failure of welded specimen in tensile tests envisaged the fact in present investigation. Stress relief annealing shifted the failure prone area away from FB-1, where heterogeneities were less. Better control thus could be made with annealed samples to improve the welded joint efficiency further. In this respect, heat treatment has marginal effect on IN182W. Thus, more flexibility was there to play with fabrication parameters for DMW produced with IN82.

V. CONCLUSIONS

Dissimilar metal joint between SA 508 low alloy steel and 304LN stainless steel was fabricated. IN82 and IN182 were used as buttering material and weld metal. One set of sample was stress relief annealed at ~923 K (650 °C) for 90 minutes after buttering on LAS. Other set was investigated in as-welded condition. The microstructure of different zones was studied. *In situ* deformation characteristics of miniature samples was examined in scanning electron microscope. Major observations are summarized below:

- In welded condition, LAS side contained coarse grain ferrite–pearlite structure adjacent to fusion boundary-1 and fine grain ferrite–pearlite structure between coarse grain region and base material, *i.e.*, tempered martensite. Collectively, the whole region was termed as heat-affected zone. Stress relief annealing resulted in overall increment in width of this region for both joints.
- Close to fusion boundary-1, within buttering material, discontinuous islands of martensite formed along with Type-I and II boundaries. After heat treatment, Type-I and II boundary did not change their position with respect to FB-1 significantly as they contained numerous alloy carbides, restricting their movement. Width of martensite layer was reduced after annealing as previously formed martensite was tempered.
- Fusion boundary-2 exhibited unmixed zone due to physical incompatibility between weld metal and 304LN stainless steel. Within the heat-affected zone of 304LN SS, welded specimens exhibited matrix grain growth due to thermal effect.

- In welded specimen, peak hardness was observed adjacent to FB-1, whereas annealing shifted the peak toward buttering material for both welds. Peak hardness near FB-1 was attributed to martensite and tiny complex alloy carbide formation. Shifting of peak in microhardness profile was ascribed to fine cementite distribution accompanied by freshly formed martensite away from interface.
- In as welded condition, stress concentration site was near FB-1 and crack initiated from that location. After heat treatment, the same location moved toward buttering material; hence, crack started appearing away from FB-1. Failure was always through buttering material, as it was the weakest region across weld line.
- Joints fabricated with IN82 consumable, exhibited better bond strength than the joint produced with IN182 in as welded condition. Heat treatment decreased bond strength, and the reduction was maximum for IN82HT.

ACKNOWLEDGMENTS

The authors are indebted to the Director, CSIR-NML for providing infrastructural facilities to carry out the investigation and providing permission to publish the work. One of the authors would also like to thank faculties of the National Institute of Technology, Tiruchirapalli, for providing valuable suggestions at various phases of the work.

REFERENCES

1. A. Celik and A. Alsaran: *Mater. Charact.*, 1999, vol. 43, pp. 311–18.
2. M. Sireesha, S.K. Albert, V. Shankar, and S. Sundaresan: *J Nucl. Mater.*, 2000, vol. 279, pp. 65–76.
3. D. Rathod, S. Aravindan, P.K. Singh, and S. Pandey: *ISIJ Int.*, 2014, vol. 54, pp. 1866–75.
4. A.M. Shariatpanahi and H. Farhangi: *Adv. Mater. Res.*, 2010, vols. 83–86, pp. 449–56.
5. J.W. Kim, K. Lee, J.S. Kim, and T.S. Byun: *J. Nucl. Mater.*, 2009, vol. 384, pp. 212–21.
6. M. Ghosh, R. Santosh, S.K. Das, G. Das, B. Mahato, J. Korody, S. Kumar, and P.K. Singh: *Metal. Mater. Trans. A*, 2015, vol. 46A, pp. 3555–68.
7. R. Viswanathan, R.I. Jaffee, and J. Dimmer: *Proceedings of Conference on Joining Dissimilar Metals*, 1982.
8. H.P. Seifert, S. Ritter, T. Shoji, Q.J. Peng, Y. Takeda, and Z.P. Lu: *J. Nucl. Mater.*, 2008, vol. 378, pp. 197–210.
9. R.D. Nicholson: *Metals Technol.*, 1982, vol. 9, pp. 305–11.
10. W.K.C. Jones and P.J. Alberry: Model for stress accumulation in steels during welding. *Proceedings of the Conference on Residual Stresses in Welded Construction and Their Effects*, 1978.
11. K. Gokul Kumar, K.D. Ramkumar, and N. Arivazhagan: *J. Mech. Sci. Technol.*, 2015, vol. 29, pp. 1039–47.
12. USNRC. Crack in weld area of reactor coolant system hot leg piping at VC Summer, IN00-17, October 18, 2000.
13. M.K. Samal, M. Seidenfuss, E. Roos, and K. Balani: *Eng. Fail. Anal.*, 2011, vol. 18, pp. 999–1008.
14. J.N. Dupont and C.S. Kusko: *Weld. J. N. Y.*, 2007, vol. 86, pp. 51–54.
15. R. Mittal and B.S. Sidhu: *J. Mater. Process. Technol.*, 2015, vol. 220, pp. 76–86.

16. C Jang, J Lee, JS Kim, and TE Jin: *Int. J. Press. Vessels Pip.*, 2008, vol. 85, pp. 635–46.
17. H. Ming, Z. Zhang, J. Wang, E.H. Han, and W. Ke: *Mats Charac.*, 2014, vol. 97, pp. 101–15.
18. C. Pan and Z. Zhang: *Mater. Charact.*, 1996, vol. 36, pp. 5–10.
19. G Cam, C Yeni, S Erim, V Ventzke, and M Kocak: *Sci. Technol. Weld. Join.*, 1998, vol. 3, pp. 177–89.
20. G Cam, S Erim, C Yeni, and M Kocak: *Weld. Res. Suppl.*, 1999, vol. 78, pp. 193s–201s.
21. G. Cam: *Int. Mater. Rev.*, 2011, vol. 56, pp. 1–48.
22. D.C. Zipperian: Metallographic specimen preparation basics. <http://www.metallographic.com/Technical/Basics.pdf>.
23. JN DuPont, JN Lippold, and SD Kiser: *Welding Metallurgy and Weldability of Ni-Base Alloys*, Wiley, Hoboken, 2009, pp. 327–76 Chap. 7.
24. H.S. Hosseini, M. Shamanian, and A. Kermanpur: *Mater. Charact.*, 2011, vol. 62, pp. 425–31.
25. D.A. Curry: *Met. Sci.*, 1984, vol. 18, pp. 67–76.
26. N. Jia, P. Eisenlohr, F. Roters, D. Raabe, and X. Zhao: *Acta Mater.*, 2012, vol. 60, pp. 3415–34.
27. S Missori and C Koerber: *Weld. J. Incl. Weld. Res. Suppl.*, 1997, vol. 76, pp. 125–34.
28. L. Yang, X. Dang, M. Li, and N. Ji: *Proceedings of 2nd International Conference on Electronic and Mechanical Engineering and Information Technology (EMEIT 2012)*, Shenyang Liaoning, China, B. Wu, eds., Atlantis Press, Paris, pp. 697–700.
29. TW Nelson, JC Lippold, and MJ Mills: *Weld. J. N. Y.*, 1999, vol. 78, pp. 329–37.
30. Y.L. Shen: *Scr. Mater.*, 1991, vol. 25, pp. 1081–85.
31. H. Naffakh, M. Shamanian, and F. Ashrafzadeh: *J. Mater. Process. Technol.*, 2009, vol. 209, pp. 3628–39.